Editors' Suggestion

Topological Phononic Logic

Harris Pirie,[1] Shuvom Sadhuka,[2] Jennifer Wang,[2,3] Radu Andrei,[1] and Jennifer E. Hoffman[1,2,*]
[1]*Department of Physics, Harvard University, Cambridge, Massachusetts 02138, USA*
[2]*School of Engineering and Applied Science, Harvard University, Cambridge, Massachusetts 02138, USA*
[3]*Department of Physics, Wellesley College, Wellesley, Massachusetts 02481, USA*

(Received 1 April 2019; accepted 15 November 2021; published 5 January 2022)

Topological metamaterials have robust properties engineered from their macroscopic arrangement, rather than their microscopic constituency. They can be designed by starting from Dirac metamaterials with either symmetry-enforced or accidental degeneracy. The latter case provides greater flexibility in the design of topological switches, waveguides, and cloaking devices, because a large number of tuning parameters can be used to break the degeneracy and induce a topological phase. However, the design of a topological logic element—a switch that can be controlled by the output of a separate switch—remains elusive. Here we numerically demonstrate a topological logic gate for ultrasound by exploiting the large phase space of accidental degeneracies in a honeycomb lattice. We find that a degeneracy can be broken by six physical parameters, and we show how to tune these parameters to create a phononic switch that transitions between a topological waveguide and a trivial insulator by ultrasonic heating. Our design scheme is directly applicable to photonic crystals and may guide the design of future electronic topological transistors.

DOI: 10.1103/PhysRevLett.128.015501

Topological insulators were first conceived as quantum electronic materials with an insulating bulk and conducting surface Dirac states, allowing for dissipationless charge and spin transport along their boundaries. Their central principle—the inversion of energy bands—is also present in many classical lattice systems, inspiring the design of photonic [1–3], phononic [4], and mechanical metamaterials [5–7] with topologically protected transport. These classical systems provide a platform to test ideas in topological band theory, because they are more tangibly understood than their quantum counterparts, and their governing wave equations can be solved exactly. Their robust properties have been used in many promising applications including zero- and negative-refractive-index materials [8–12], cloaking [13,14], and protected waveguides for sound and light that outperform nontopological alternatives [15–17]. A key remaining challenge is to control the topological phase in a way that allows waveguides to toggle one another, paving the way towards topological logic circuits with greater efficiency than current CMOS technology [18–20].

A general design approach to achieve the band inversion that defines a topological metamaterial is to start from a bulk Dirac state, then intentionally break the Dirac-point degeneracy to open a negative gap. This approach can be broadly divided into two methods. The first method starts from a symmetry-enforced Dirac state, such as the K-point Dirac cone in graphenelike honeycomb or triangular metamaterials, then opens a gap by breaking a symmetry of the system. In systems with broken time-reversal ($\mathcal{T}$) symmetry [21–25], the resultant topological phase is analogous to the quantum Hall effect, while those with broken inversion symmetry [26–31] can realize an analog of the quantum spin Hall effect. However, there is limited flexibility in the design of these topological phases, as they can be tuned only by a symmetry-breaking operation. On the other hand, the second method searches for the accidental degeneracy of three [8,14,32] or four [9,33,34] bands, producing a Dirac-like cone or double Dirac cones, respectively. This method gives access to a far larger set of topological phases because the accidental degeneracy can be broken by several more-accessible tuning parameters while retaining inversion and $\mathcal{T}$ symmetry. Despite the utility and flexibility of this second method, the complete space of all topological phases has yet to be mapped for any accidental degeneracy.

We start from a particular accidental bulk Dirac-point degeneracy that gives rise to a topological state analogous to a quantum spin Hall system. In a quantum spin Hall system, the protection of the Dirac point is a consequence of the spin-½ nature of electrons. Specifically, because $\mathcal{T}^2 = -1$ for spin-½ states, Kramers theorem requires a degeneracy at all $\mathcal{T}$-invariant points of the Brillouin zone. However, spin-0 phononic and spin-1 photonic systems both have $\mathcal{T}^2 = +1$, so Kramers theorem does not apply. Instead, designs typically rely on mode hybridization to form a pseudospin-½ subsystem, for example with the transverse electric and magnetic polarizations of light [2]. But transverse shear modes are not available in airborne acoustics, so finding an analogy of Kramers theorem is challenging. In 2012, Sakoda [33] addressed this issue and constructed a pseudospin-½ system using the discrete symmetries of a triangular lattice, which was adapted to longitudinal acoustic modes shortly thereafter [9,34,35], and subsequently demonstrated experimentally [16]. In this scheme, a lattice with C_{6v} symmetry generates an accidental degeneracy at the Γ point between doubly degenerate E_1 and E_2 modes that transform as (x, y) and $(xy, x^2 - y^2)$, denoted (p_x, p_y) and $(d_{xy}, d_{x^2-y^2})$, respectively. These doubly degenerate modes allow the formation of a pseudospin-1/2 basis, with corresponding eigenstates $p_\pm = (p_x \pm ip_y)/\sqrt{2}$ and $d_\pm = (d_{x^2-y^2} \pm id_{xy})/\sqrt{2}$. The accidental degeneracy between the $p_\pm$ and $d_\pm$ subsystems can be lifted without breaking C_{6v} symmetry, resulting in a topological phase with helical edge modes protected by a pseudo-$\mathcal{T}$ symmetry, analogous to the quantum spin Hall state [16,26].

Here we numerically investigate the topological phase space for a Γ-point accidental degeneracy in a phononic honeycomb lattice using commercial finite-element modeling software COMSOL MULTIPHYSICS. We find a manifold of system configurations that host a bulk accidental double Dirac cone, and we demonstrate that a topological phase can be induced by gapping the Dirac node with six independent physical parameters, which collapse into a three-dimensional (3D) phase space. This vast phase space guides the design of three topological circuit elements: a static-geometry waveguide, an externally switchable device, and a universal logic gate. While we illustrate each element using phononic metamaterials, the same design principles apply to electronic and photonic metamaterials.

A static-geometry topological waveguide is formed at the interface between a lattice with normally ordered bands and one with inverted bands. This type of waveguide was already demonstrated using two hexagonal phononic crystals of steel pillars in a fluid medium with different filling ratios, $\tilde{r} = R/a$ [16,34], where R and a are the radius and spacing of the pillars, respectively [see inset to Fig. 1(b)]. When the filling ratio is large, the band structure around the Γ point contains doubly degenerate $p_\pm$ modes separated from $d_\pm$ modes by a positive energy gap, $\Delta > 0$, as shown in Fig. 1(a). At the critical filling ratio for a steel and water system, $\tilde{r}^* = 0.371$, the four modes become accidentally degenerate and the bulk metamaterial hosts double Dirac cones. Below critical filling, the $p_\pm$ modes have higher energy than the $d_\pm$ modes, and the band structure contains a negative energy gap, $\Delta < 0$. Topologically protected edge modes are confined to the interface between a positive- and negative-gapped material, allowing the design of topological waveguides that are pseudospin polarized and immune to defects including cavities, bends, and lattice disorder [16].

Our first advance is a new mechanism to create an externally switchable topological waveguide for sound, providing a simple alternative to the existing schemes [36–38]. In general, a topological switch hosts robust transport when "on," but is a trivial insulator when "off." It requires a

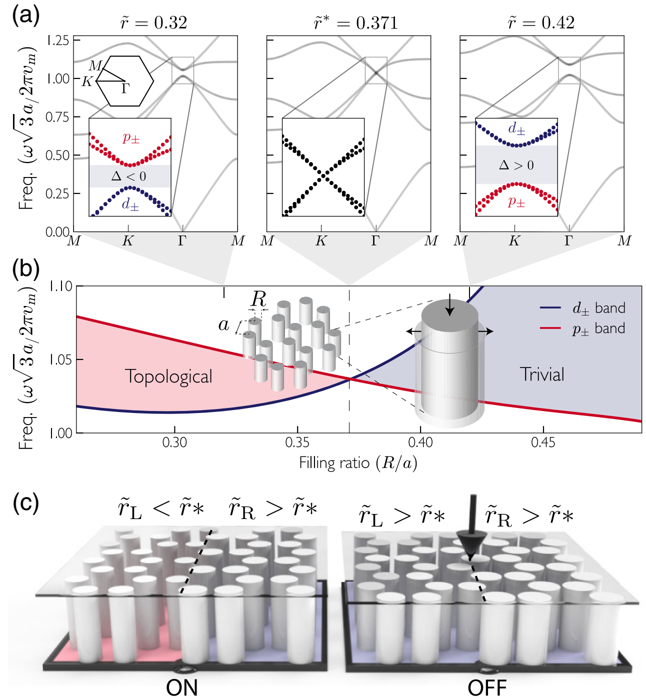

FIG. 1. An externally controlled topological switch for sound. (a) The phononic band structure for a honeycomb lattice of steel pillars in water passes through an accidental degeneracy as the radius of the pillars is varied. This degeneracy is between $p_\pm$ bands (red) and $d_\pm$ bands (blue), and occurs at the critical filling ratio of $\tilde{r}^* \equiv R^*/a = 0.371$ (middle panel). As the filling ratio is tuned away from this value, a positive (right) or negative (left) band gap opens, leading to a topological phase transition. (b) This transition can be clearly seen by tracking the Γ-point eigenvalues as $\tilde{r}$ is tuned. (c) A topological waveguide is made by placing two lattices with $\tilde{r}_L < \tilde{r}^*$ and $\tilde{r}_R > \tilde{r}^*$ next to each other (left panel). When the pillars are compressed vertically, their radius expands such that both sides of the waveguide become trivial insulators (right panel). This device is a topological switch for sound that turns off when compressed.

tuning mechanism capable of changing the sign of the band gap on the topological side, while leaving the trivial side unchanged. We found that an external vertical compression or extension can induce this behavior, as it alters the pillars' radius, which can toggle the topological phase [see inset to Fig. 1(b)]. For materials with a positive Poisson's ratio, a topological waveguide naturally switches off when compressed, once the filling ratio of its topological side increases beyond $\tilde{r}^*$, as shown in Fig. 1(c). In practice, rubber pillars are ideal for this application as they are far more stretchable than metal pillars, and have a higher Poisson's ratio [39]. Advancing beyond static-geometry topological waveguides [15–17,28–31], this type of switch could be used to control passive acoustic isolation systems, but the output of one switch cannot sustain the macroscopic stretch required to activate a second, similar switch.

Our second, more significant advance is to design a phononically controlled acoustic switch—i.e., a topological logic element. Like electronic field-effect transistors, these switches may be connected together to form circuits. Here we rely explicitly on the flexibility granted by the large phase space of accidental degeneracies in a honeycomb metamaterial. In general, an accidental band degeneracy can be lifted by tuning any lattice parameter, as it is not protected by symmetry. The relevant parameters in a phononic lattice define the acoustic wave equation,

$$\nabla \cdot \left[\frac{1}{\rho_r(\mathbf{r})}\nabla p(\mathbf{r})\right] = -\frac{\omega^2}{v_m^2}\cdot\frac{p(\mathbf{r})}{v_r^2(\mathbf{r})\rho_r(\mathbf{r})} \tag{1}$$

where p is the pressure, ω is the eigenfrequency, and $\rho_r(\mathbf{r}) = \rho(\mathbf{r})/\rho_m$ and $v_r(\mathbf{r}) = v(\mathbf{r})/v_m$ are the relative density and speed of sound, respectively. In total, there are six physical parameters that can tune the resulting eigenspectrum: R, a, ρ_p, ρ_m, v_p, and v_m, where the subscript refers to pillars or medium. First note that uniformly scaling ρ_p and ρ_m produces no change. Second, uniformly scaling v_p and v_m scales all eigenfrequencies of Eq. (1), but does not shift eigenfrequencies relative to one another, and therefore cannot alter the topological phase. We take this scaling into account by adopting dimensionless units for frequency, $\tilde{\omega} = \omega\sqrt{3}a/2\pi v_m$. In fact, the frequency-normalized band structure depends only on three dimensionless ratios: $\tilde{r} = R/a$, $\tilde{v} = v_p/v_m$, and $\tilde{\rho} = \rho_p/\rho_m$. In the example system of steel pillars in water, we find that varying either $\tilde{v}$ or $\tilde{\rho}$ lifts the accidental degeneracy and can open a negative gap [Figs. 2(a) and 2(b)]. More generally, varying any combination of lattice parameters along a path in $(\tilde{v}, \tilde{\rho}, \tilde{r})$ space that connects the topological phase to the trivial phase must pass through an accidental degeneracy. Consequently, there exists a surface in $(\tilde{v}, \tilde{\rho}, \tilde{r})$ space that separates the topological phase from the trivial phase, on which there is accidental degeneracy between $p_\pm$ and $d_\pm$ modes and a bulk double Dirac cone. We numerically calculated the shape of this surface, shown in Fig. 2(c), by recording the accidental crossing point in an $\tilde{r}$ sweep for a discrete set of $(\tilde{v}, \tilde{\rho})$ points, at fixed (v_m, ρ_m).

A key challenge in designing a topological switch is to preserve overlapping bulk spectral gaps before and after switching. For example, in the sweep shown in Fig. 2(a), increasing $\tilde{\rho}$ causes both $p_\pm$ and $d_\pm$ modes to decrease in frequency, leading to a band inversion because the $d_\pm$ modes decrease faster than the $p_\pm$ modes. Yet, this tuning parameter alone cannot be used to design a topological waveguide because at any frequency there are bulk modes in one of the two sides that mask the edge states, unlike Fig. 1(b). The same accidental degeneracy can be broken by varying $\tilde{v}$, which causes both $p_\pm$ and $d_\pm$ modes to increase in frequency [Fig. 2(b)], again precluding a usefully overlapping gap. However, an overlapping bulk gap may occur when tuning a combination of $\tilde{v}$ and $\tilde{\rho}$, for instance, in a waveguide between two sets of pillars with different materials but the same radius. In general, each accidental degeneracy on the surface in Fig. 2(c) can be used to construct a practical waveguide for a parameter sweep through some solid angle in $(\tilde{v}, \tilde{\rho}, \tilde{r})$ space. Schematically, such a waveguide combines two points in parameter space connected by a path that punctures the surface in Fig. 2(c). Similarly, a topological switch combines four points in phase space, with three above the surface (trivial) and one below (topological), e.g., the square points in Fig. 2(c). Furthermore, a useful switch requires the bulk to remain gapped and overlapping on all four $(\tilde{v}, \tilde{\rho}, \tilde{r})$ trajectories that connect these points, except where they pass through the surface.

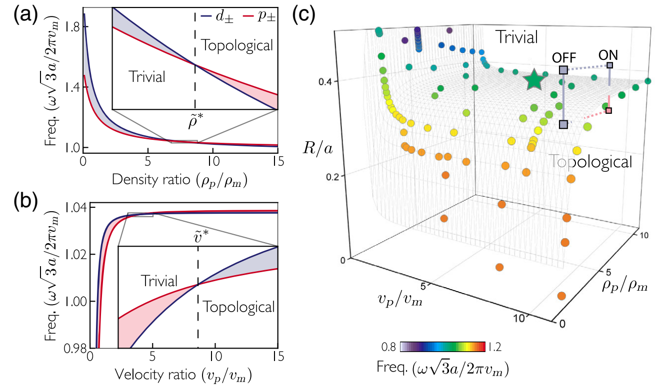

FIG. 2. Topological phase space for a honeycomb phononic lattice. An accidental degeneracy between the $p_\pm$ and $d_\pm$ modes in a steel and water system [green star in (c)] can be broken by tuning the ratio of (a) density while holding speed of sound and radius fixed; or (b) speed of sound while holding radius and density fixed. (c) Each accidental degeneracy is a point in $(\tilde{v}, \tilde{\rho}, \tilde{r})$ space, colored according to its crossing frequency (e.g., the steel and water system has a crossing frequency of 90 kHz for $a = 1$ cm). Together, they separate phase space into a topological and a trivial region. A topological waveguide pairs configurations from different sides of this surface (see solid line labeled ON), provided their bulk spectral gaps overlap. Transmission through it can be switched off by tuning to two configurations that occur on the same side of the surface (see path labeled OFF).

To enable the output of one switch to control the next, our design for a phononically controlled topological switch uses a temperature increase delivered by ultrasonic phonons as its tuning mechanism. Each switch contains a honeycomb lattice of steel pillars connecting the source and drain terminals, attached to a base plate made from a second material, in an air-tight container, as shown in Fig. 3(c). The temperature increase needed to toggle the switch is provided by a thermoacoustic converter connected to a third terminal [labeled "gate" in Figs. 4(g) and 4(h), see [39]]. The primary effect of heating the device is to change the speed of sound in the medium, which typically increases all eigenfrequencies of the system [see dashed

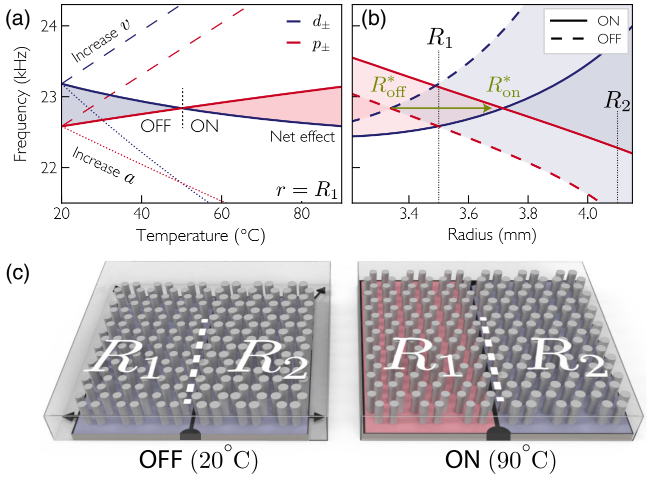

FIG. 3. Designing a temperature-controlled topological switch. We consider a honeycomb lattice of steel pillars ($R_1 = 3.5$ mm, $R_2 = 4.1$ mm, $a = 8.5$ mm) anchored to a high-thermal-expansion base plate, in an air medium within a sealed fixed-size box. (a) Heating this system has two main competing effects: eigenfrequencies are increased by raising the speed of sound in air (dashed lines), but decreased as the base plate thermally expands (dotted lines). The latter effect also tunes $\tilde{r}$ to induce a band inversion. These two effects can be balanced by correctly choosing the thermal expansion coefficient of the base plate (here $1.61 \times 10^{-3}\ \mathrm{K}^{-1}$), providing a temperature-tunable topological phase transition with an overlapping spectral gap (solid lines). (b) A topological switch combines two sizes of pillars: one side transitions from trivial to topological as the switch is heated (R_1), while the other remains trivial throughout (R_2). (c) Unlike the switch design in Fig. 1(c), which is triggered by tuning R at fixed a, this switch is turned on by increasing a at fixed R, and can be actuated by phonon-delivered heat.

lines in Fig. 3(a)]. Second, heating causes thermal expansion of the materials, increasing both R and a, though not necessarily equally. If the base plate and pillar materials are selected such that a increases faster than R, the net result is to reduce all eigenfrequencies of the system and induce a band inversion [dotted lines in Fig. 3(a)]. Finally, heating alters the density of the air and the materials, which has been taken into account, but is insignificant. The first two effects can be balanced to maintain a bulk gap throughout the switching process, by fixing the ratio v_m/a that appears in the eigenfrequency of Eq. (1). Because the base plate expands linearly with temperature, we seek a medium where v_m also increases linearly. For an ideal gas at temperature T, v_m increases as $\sqrt{T}$, but the trend is almost linear near room temperature; as such, air is a suitable medium. Consequently, to keep v_m/a fixed as the temperature increases from T_i to T_f, we seek a base material with a coefficient of thermal expansion given by $\alpha = 1/(T_i + \sqrt{T_i T_f})$. For the proof-of-principle switch shown in Fig. 3(b), the required base-plate thermal expansion coefficient is $1.61 \times 10^{-3}\ \mathrm{K}^{-1}$, which is within

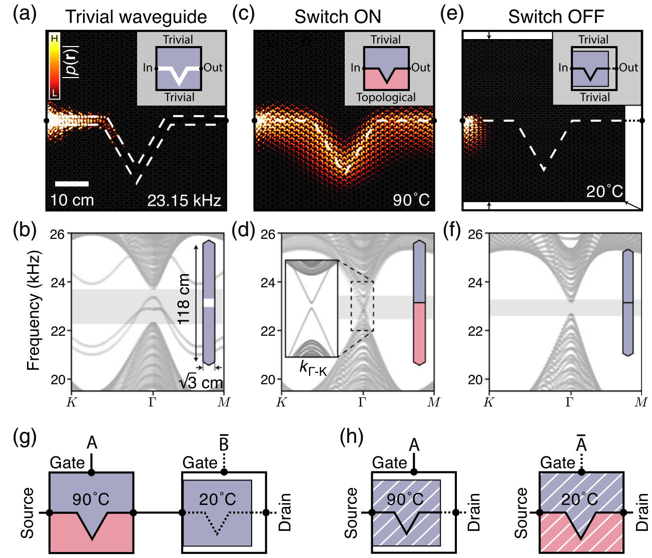

FIG. 4. Topological logic gates with ultrasound. (a) Transmission through a trivial waveguide, like this channel in an insulating steel-and-air phononic crystal, is disrupted by disorder and bends. (b) The band structure of the corresponding supercell (see inset) contains a bulk gap with trivial edge states. (c) In contrast, a topological waveguide with the same parameters as in Fig. 3, allows robust transport regardless of channel geometry; it can be used as the on state of a topological switch. (d) Its band structure hosts protected, Dirac-like edge states (inset) due to a negative bulk gap on one side. (e) When the system is cooled, it contracts and both sides become trivial insulators, preventing transmission. (f) Excitations at frequencies within the gap decay exponentially as they enter the device. (g) A topological AND gate, constructed from two switches in series, requires both control signals (A and B) to be high to register an output. (h) A topological NOT gate uses a base plate with a negative thermal expansion coefficient; it contracts to turn off when heated (left), and expands to turn on when cooled (right).

the range achievable by origami metamaterials [44]. Alternatively, we empirically demonstrated an even larger effective thermal expansion coefficient by thermally actuating using the shape-memory alloy Nitinol [39].

The advantage of a topological phononic switch can be seen from the finite-sized calculations in Fig. 4. Unlike a trivial waveguide, which experiences significant losses induced by disorder and bends [Fig. 4(a) and 4(b)], the topological switch acts as a robust pseudospin-dependent waveguide when on due to a Dirac cone between the two sides [Figs. 4(c) and 4(d)]. As it is cooled, the pillars contract around the input terminal; both sides become trivially insulating and block transmission, turning the switch off [Figs. 4(e) and 4(f)]. Our topological switch is stable against mild temperature changes provided its operational frequency remains within the spectral gap [see Fig. 3(a)]. Such temperature variations alter only the localization of the edge states, not their presence or absence [39].

Our proof-of-principle temperature-controlled phononic switches can be linked to form a universal NAND gate with two main segments. First, we design a topological AND gate by connecting two switches in series [Fig. 4(g)]. This device requires both control signals (A and B) to be on to heat each switch and allow information to propagate [39]. Second, to design a topological NOT gate, we utilize a base plate material that has a negative coefficient of thermal expansion; that is, it shrinks when heated. At room temperature (control is off), the NOT gate is a topological waveguide that transmits information, but when the control is on, the device heats and shrinks, transitioning to a trivial insulator. To maintain an overlapping bulk gap throughout this transition, we require a medium where the speed of sound decreases with increasing temperature, a behavior commonly observed in oils [45]. Specifically, a device using steel pillars in sunflower oil requires a coefficient of thermal expansion of $-2.0 \times 10^{-3}\ \mathrm{K}^{-1}$ to keep the ratio v_m/a fixed, a value recently demonstrated [44].

The design of topological metamaterials based on a broken accidental degeneracy is extremely versatile due to the large number of tuning parameters available. Specifically, for a phononic honeycomb lattice, the topological phase can be tuned by six independent parameters, which collapse onto a 3D phase space. This phase space guided a proof-of-principle design for a phononically controlled topological switch, the building block of an acoustic logic gate. The macroscopic size and moderate speed of our device makes it an ideal tool for teaching and understanding topological materials. More importantly, the same design process can be followed for piezoelectric materials at mesoscopic length scales, enabling switchable control of topologically protected surface-acoustic waves for integrated phononics [46]. Finally, our approach directly applies to optical systems under a simple mapping of variables [32], or to nanostructured quantum materials [47], providing a new direction for developing a field-effect topological transistor.

We thank Katia Bertoldi, Barbara Dorritie, Jason Hoffman, David Lee, Ciarán O'Neill, Ben November, Pai Wang, and Jack Zhang for helpful conversations. This work was supported by the Science and Technology Center for Integrated Quantum Materials under the National Science Foundation Grant No. DMR-1231319.

[*]jhoffman@physics.harvard.edu

[1] F. D. M. Haldane and S. Raghu, Possible Realization of Directional Optical Waveguides in Photonic Crystals with Broken Time-Reversal Symmetry, Phys. Rev. Lett. **100**, 013904 (2008).

[2] A. B. Khanikaev, S. H. Mousavi, W.-K. Tse, M. Kargarian, A. H. MacDonald, and G. Shvets, Photonic topological insulators, Nat. Mater. **12**, 233 (2013).

[3] L. Lu, J. D. Joannopoulos, and M. Soljačić, Topological photonics, Nat. Photonics **8**, 821 (2014).

[4] H. Ge, M. Yang, C. Ma, M.-H. Lu, Y.-F. Chen, N. Fang, and P. Sheng, Breaking the barriers: Advances in acoustic functional materials, Natl. Sci. Rev. **5**, 159 (2018).

[5] C. L. Kane and T. C. Lubensky, Topological boundary modes in isostatic lattices, Nat. Phys. **10**, 39 (2014).

[6] R. Süsstrunk and S. D. Huber, Observation of phononic helical edge states in a mechanical topological insulator, Science **349**, 47 (2015).

[7] S. D. Huber, Topological mechanics, Nat. Phys. **12**, 621 (2016).

[8] F. Liu, X. Huang, and C. T. Chan, Dirac cones at $\vec{k} = 0$ in acoustic crystals and zero refractive index acoustic materials, Appl. Phys. Lett. **100**, 071911 (2012).

[9] Y. Li, Y. Wu, and J. Mei, Double Dirac cones in phononic crystals, Appl. Phys. Lett. **105**, 014107 (2014).

[10] M. Dubois, C. Shi, X. Zhu, Y. Wang, and X. Zhang, Observation of acoustic Dirac-like cone and double zero refractive index, Nat. Commun. **8**, 14871 (2017).

[11] I. Liberal and N. Engheta, Near-zero refractive index photonics, Nat. Photonics **11**, 149 (2017).

[12] H. He, C. Qiu, L. Ye, X. Cai, X. Fan, M. Ke, F. Zhang, and Z. Liu, Topological negative refraction of surface acoustic waves in a Weyl phononic crystal, Nature (London) **560**, 61 (2018).

[13] J. Hao, W. Yan, and M. Qiu, Super-reflection and cloaking based on zero index metamaterial, Appl. Phys. Lett. **96**, 101109 (2010).

[14] X. Huang, Y. Lai, Z. H. Hang, H. Zheng, and C. T. Chan, Dirac cones induced by accidental degeneracy in photonic crystals and zero-refractive-index materials, Nat. Mater. **10**, 582 (2011).

[15] S. H. Mousavi, A. B. Khanikaev, and Z. Wang, Topologically protected elastic waves in phononic metamaterials, Nat. Commun. **6**, 8682 (2015).

[16] C. He, X. Ni, H. Ge, X.-C. Sun, Y.-B. Chen, M.-H. Lu, X.-P. Liu, and Y.-F. Chen, Acoustic topological insulator and robust one-way sound transport, Nat. Phys. **12**, 1124 (2016).

[17] Q. Wei, Y. Tian, S.-Y. Zuo, Y. Cheng, and X.-J. Liu, Experimental demonstration of topologically protected efficient sound propagation in an acoustic waveguide network, Phys. Rev. B **95**, 094305 (2017).

[18] J. G. Checkelsky, J. Ye, Y. Onose, Y. Iwasa, and Y. Tokura, Dirac-fermion-mediated ferromagnetism in a topological insulator, Nat. Phys. **8**, 729 (2012).

[19] L. A. Wray, Topological transistor, Nat. Phys. **8**, 705 (2012).

[20] J. L. Collins, A. Tadich, W. Wu, L. C. Gomes, J. N. B. Rodrigues, C. Liu, J. Hellerstedt, H. Ryu, S. Tang, S.-K. Mo, S. Adam, S. A. Yang, M. S. Fuhrer, and M. T. Edmonds, Electric-field-tuned topological phase transition in ultrathin Na_3Bi, Nature (London) **564**, 390 (2018).

[21] Z. Wang, Y. Chong, J. D. Joannopoulos, and M. Soljačić, Observation of unidirectional backscattering-immune topological electromagnetic states, Nature (London) **461**, 772 (2009).

[22] R. Fleury, D. L. Sounas, C. F. Sieck, M. R. Haberman, and A. Alù, Sound isolation and giant linear nonreciprocity in a compact acoustic circulator, Science **343**, 516 (2014).

[23] Z. Yang, F. Gao, X. Shi, X. Lin, Z. Gao, Y. Chong, and B. Zhang, Topological Acoustics, Phys. Rev. Lett. **114**, 114301 (2015).

[24] P. Wang, L. Lu, and K. Bertoldi, Topological Phononic Crystals with One-Way Elastic Edge Waves, Phys. Rev. Lett. **115**, 104302 (2015).

[25] L. M. Nash, D. Kleckner, A. Read, V. Vitelli, A. M. Turner, and W. T. M. Irvine, Topological mechanics of gyroscopic metamaterials, Proc. Natl. Acad. Sci. U.S.A. **112**, 14495 (2015).

[26] L.-H. Wu and X. Hu, Scheme for Achieving a Topological Photonic Crystal by Using Dielectric Material, Phys. Rev. Lett. **114**, 223901 (2015).

[27] Z. Zhang, Q. Wei, Y. Cheng, T. Zhang, D. Wu, and X. Liu, Topological Creation of Acoustic Pseudospin Multipoles in a Flow-Free Symmetry-Broken Metamaterial Lattice, Phys. Rev. Lett. **118**, 084303 (2017).

[28] Z. Zhang, Y. Tian, Y. Cheng, X. Liu, and J. Christensen, Experimental verification of acoustic pseudospin multipoles in a symmetry-broken snowflakelike topological insulator, Phys. Rev. B **96**, 241306(R) (2017).

[29] Y. Deng, H. Ge, Y. Tian, M. Lu, and Y. Jing, Observation of zone folding induced acoustic topological insulators and the role of spin-mixing defects, Phys. Rev. B **96**, 184305 (2017).

[30] Y. Yang, Y. F. Xu, T. Xu, H.-X. Wang, J.-H. Jiang, X. Hu, and Z. H. Hang, Visualization of a Unidirectional Electromagnetic Waveguide Using Topological Photonic Crystals Made of Dielectric Materials, Phys. Rev. Lett. **120**, 217401 (2018).

[31] B.-Z. Xia, T.-T. Liu, G.-L. Huang, H.-Q. Dai, J.-R. Jiao, X.-G. Zang, D.-J. Yu, S.-J. Zheng, and J. Liu, Topological phononic insulator with robust pseudospin-dependent transport, Phys. Rev. B **96**, 094106 (2017).

[32] J. Mei, Y. Wu, C. T. Chan, and Z.-Q. Zhang, First-principles study of Dirac and Dirac-like cones in phononic and photonic crystals, Phys. Rev. B **86**, 035141 (2012).

[33] K. Sakoda, Double Dirac cones in triangular-lattice metamaterials, Opt. Express **20**, 9925 (2012).

[34] Z.-G. Chen, X. Ni, Y. Wu, C. He, X.-C. Sun, L.-Y. Zheng, M.-H. Lu, and Y.-F. Chen, Accidental degeneracy of double Dirac cones in a phononic crystal, Sci. Rep. **4**, 4613 (2015).

[35] J. Mei, Z. Chen, and Y. Wu, Pseudo-time-reversal symmetry and topological edge states in two-dimensional acoustic crystals, Sci. Rep. **6**, 32752 (2016).

[36] R. Süsstrunk, P. Zimmermann, and S. D. Huber, Switchable topological phonon channels, New J. Phys. **19**, 015013 (2017).

[37] Z. Zhang, Y. Tian, Y. Cheng, Q. Wei, X. Liu, and J. Christensen, Topological Acoustic Delay Line, Phys. Rev. Applied **9**, 034032 (2018).

[38] J.-P. Xia, D. Jia, H.-X. Sun, S.-Q. Yuan, Y. Ge, Q.-R. Si, and X.-J. Liu, Programmable coding acoustic topological insulator, Adv. Mater. **30**, 1805002 (2018).

[39] See Supplemental Materials at http://link.aps.org/supplemental/10.1103/PhysRevLett.128.015501 for the design of a rubber waveguide, a thermoacoustic converter, an expandable base plate, and a lower-power logic gate; calculations of two connected switches at different temperatures; and a discussion of materials selection and the robustness of the edge states, containing Refs. [40–43].

[40] O. Symko, E. Abdel-Rahman, Y. Kwon, M. Emmi, and R. Behunin, Design and development of high-frequency thermoacoustic engines for thermal management in microelectronics, Microelectron. J. **35**, 185 (2004).

[41] G. Chen, L. Tang, B. Mace, and Z. Yu, Multi-physics coupling in thermoacoustic devices: A review, Renew. Sustain. Energy Rev. **146**, 111170 (2021).

[42] B. B. S. T. Boonstra, Stress-strain properties of natural rubber under biaxial strain, J. Appl. Phys. **21**, 1098 (1950).

[43] B. A. Bernevig, T. L. Hughes, and S.-C. Zhang, Quantum spin hall effect and topological phase transition in HgTe quantum wells, Science **314**, 1757 (2006).

[44] E. Boatti, N. Vasios, and K. Bertoldi, Origami metamaterials for tunable thermal expansion, Adv. Mater. **29**, 1700360 (2017).

[45] P. A. Oliveira, R. M. B. Silva, G. C. Morais, A. V. Alvarenga, and R. P. B. C. Félix, Speed of sound as a function of temperature for ultrasonic propagation in soybean oil, J. Phys. **733**, 012040 (2016).

[46] S.-Y. Yu, X.-C. Sun, X. Ni, Q. Wang, X.-J. Yan, C. He, X.-P. Liu, L. Feng, M.-H. Lu, and Y.-F. Chen, Surface phononic graphene, Nat. Mater. **15**, 1243 (2016).

[47] M. Polini, F. Guinea, M. Lewenstein, H. C. Manoharan, and V. Pellegrini, Artificial honeycomb lattices for electrons, atoms and photons, Nat. Nanotechnol. **8**, 625 (2013).